High-k Hf-based layers grown by RF magnetron sputtering

Larysa Khomenkova, C. Dufour, Pierre-Eugène Coulon, Caroline Bonafos, F. Gourbilleau

▶ **To cite this version:**

Larysa Khomenkova, C. Dufour, Pierre-Eugène Coulon, Caroline Bonafos, F. Gourbilleau. High-k Hf-based layers grown by RF magnetron sputtering. Nanotechnology, 2010, 21 (9), 10.1088/0957-4484/21/9/095704 . hal-01820398

HAL Id: hal-01820398
https://hal.science/hal-01820398v1

Submitted on 21 Jun 2018

HAL is a multi-disciplinary open access archive for the deposit and dissemination of scientific research documents, whether they are published or not. The documents may come from teaching and research institutions in France or abroad, or from public or private research centers.

L'archive ouverte pluridisciplinaire **HAL**, est destinée au dépôt et à la diffusion de documents scientifiques de niveau recherche, publiés ou non, émanant des établissements d'enseignement et de recherche français ou étrangers, des laboratoires publics ou privés.

High-*k* Hf-based layers grown by RF magnetron sputtering

L Khomenkova[1,3], C Dufour[1], P-E Coulon[2], C Bonafos[2] and F Gourbilleau[1,3]

[1] CIMAP, UMR CEA/CNRS/ENSICAEN/Université de Caen, 6 boulevard Marechal Juin, F-14050 Caen Cedex 4, France
[2] CEMES/CNRS, 29 rue Jeanne Marvig, F-31055 Toulouse, France

E-mail: larysa.khomenkova@ensicaen.fr and fabrice.gourbilleau@ensicaen.fr

Abstract

Structural and chemical properties of Hf-based layers fabricated by RF magnetron sputtering were studied by means of x-ray diffraction, transmission electron microscopy and attenuated total reflection infrared spectroscopy versus the deposition parameters and annealing treatment. The deposition and post-deposition conditions allow us to control the temperature of the amorphous–crystalline phase transition of HfO_2-based layers. It was found that silicon incorporation in an HfO_2 matrix plays the main role in the structural stability of the layers. It allows us not only to decrease the thickness of the film/substrate interfacial layer to 1 nm, but also to conserve the amorphous structure of the layers after an annealing treatment up to 900–1000 °C.

1. Introduction

Pure silicon oxide and the related oxynitrides have met their fundamental limits as conventional gate dielectrics. This gave an impulse to numerous investigations of the group IVB metal oxides (MO_2 (M = Ti, Zr, Hf)) and their solid solutions [1–8]. These high-*k* oxides are promising for future CMOS devices due to a wide bandgap (higher than 5 eV) as well as thermal stability on silicon and a high permittivity ($\varepsilon_r \geqslant 20$), which is the most important point to circumvent the problem of high leakage current. Based on thermodynamic studies [9] and bandgap measurements [10], hafnium oxide was considered as the best candidate among high-*k* dielectrics to replace SiO_2. However, in the ultrathin film approach, the structure and the properties of HfO_2 layers depend strongly on the technique used for layer fabrication, the deposition conditions and post-annealing treatment.

The widespread techniques used for fabrication of ultrathin HfO_2-based layers are vapor-based approaches such as atomic layer deposition [7, 11–13] or chemical vapor deposition [14, 15]. In most cases, the layers are grown at high temperatures (350–450 °C). At the same time, low-temperature techniques such as physical vapor deposition [16], and DC and/or RF magnetron sputtering [17–20] are not commonly addressed. Magnetron-sputtered HfO_2 layers have often been deposited from a pure metallic Hf cathode in argon plasma and then submitted to an oxidation process. A reactive sputtering of metallic Hf in an argon–oxygen gas mixture was also used to grow directly HfO_2 layers [17]. Only in a few cases were the layers grown by reactive sputtering of a pure HfO_2 target [18–20].

A clear goal of any potential high-*k* gate dielectric is to attain a sufficiently high-quality interface with the Si channel accompanied by a conservation of the amorphous structure of the gate oxide during post-deposition treatment. Unfortunately high-*k* oxides have a low crystallization temperature, whereas the stability as a single amorphous phase up to 800–1000 °C is required by CMOS thermal processing [4]. Such a requirement is coming from the fact that grain boundaries act as diffusion paths for dopants or oxygen towards the film/substrate interface. Thus, from a technological point of view, the advantages of the amorphous layers by comparison to polycrystalline gate dielectric films are a lower leakage current, a better homogeneity and, at the end, a higher reproducibility for the electrical properties. However, up to

[3] Authors to whom any correspondence should be addressed.

now, the correlation between the structure of the gate dielectric and device performance requires detailed investigation.

The use of HfO_2 as a gate dielectric suffers from the undesirable formation of a film/substrate interfacial SiO_2 layer either during deposition on the Si substrate or after post-annealing treatment [3, 4]. A lot of effort was devoted to overcome this problem and to prevent a chemical reaction between the deposited HfO_2 layer and the Si substrate. It was proposed to form oxynitrides and/or nitride barriers between the high-k material and the Si substrate. Besides, an incorporation of nitrogen into the high-k matrix during the deposition or due to post-deposition processing was found to result in the formation of HfON [17], which demonstrated thermal stability up to 1000 °C [21]. On the other hand, an incorporation of silicon into the high-k matrix results in the formation of a pseudobinary alloy such as $(MO_2)_x(SiO_2)_{1-x}$ (M = Ti, Zr, Hf) [3]. It is obvious that such an alloy has inevitably lower permittivity than that of the pure metal oxide, but it allows us to decrease the leakage current and to grow a thermodynamically stable film on the Si substrate [1, 2, 6, 22].

The analysis of the phase diagram of Ti–Si–O and Zr-Si–O systems showed that, in contrary to the Ti–Si–O system, ZrO_2 as well as its silicate (in a large phase field of the $(ZrO_2)_x(SiO_2)_{1-x}$ compositions) are both stable in direct contact with the Si substrate. Unfortunately theoretical considerations as well as experimental data are lacking for $(HfO_2)_x(SiO_2)_{1-x}$. However, based on the similarity of chemical properties of Zr and Hf ions, as well as on the available data for HfO_2 and $HfSiO_4$ materials, it is supposed that a large range of $(HfO_2)_x(SiO_2)_{1-x}$ compositions will exhibit an amorphous phase which will be thermodynamically stable up to high temperatures [6].

In the present study, pure and N-rich HfO_2-based layers have been fabricated by RF magnetron sputtering of a pure HfO_2 target in a pure argon or argon–nitrogen plasma. The Si-rich layers were grown by co-sputtering of an HfO_2 cathode topped by Si chips. The effects of the deposition parameters as well as of the annealing treatment have been analyzed by means of x-ray diffraction, infrared absorption spectroscopy and high resolution transmission electron microscopy.

This paper is organized as follows. At the beginning, the properties of pure or N-rich HfO_2 layers versus different deposition conditions and post-deposition processing will be presented. Then, the effect of silicon incorporation into the HfO_2 matrix on the HfSiO and HfSiON layers' structure will be described. Finally, the variation of the properties of Si-rich HfO_2 layers with the annealing treatment will be analyzed to demonstrate the ways to improve the thermal stability of the amorphous layer.

2. Experimental details

The layers were grown on B-doped Si substrates with a resistivity of 15 Ω cm and (100) orientation. The substrates were cleaned in a diluted hydrofluoric solution (10%) to remove the native oxide. After cleaning and drying in a nitrogen flow, the substrates were immediately placed into the vacuum preparation chamber of the deposition set-up.

Table 1. Deposition and post-deposition conditions.

Parameter	Range of variation
RF power applied on HfO_2 (RFP) (W cm^{-2})	0.48–0.98
Temperature of substrate (T_S) (°C)	45–500
Total pressure in chamber (P_{total}) (mbar)	0.04
Nitrogen partial pressure (P_N) (mbar)	0.005–0.02
Annealing temperature (T_A) (°C)	600–1100
Annealing time (t_A) (min)	5–60
Silicon surface ratio (R_{Si}) (%)	3–12

Pure and N-rich HfO_2 layers were grown by RF magnetron sputtering of a 4 inch HfO_2 target (99.9%). The main contaminant was Zr (250 ppm) while the total content of the other detected impurities (W, Fe, Ti, Mo, Mg, Ca, Cr) was 170 ppm. The layers were fabricated at different RF power densities (RFP) and substrate temperatures (T_S) in pure argon or mixed argon–nitrogen plasma. The purity of both gases was 99.9999%. The deposition time was chosen to grow films having the same thickness. The substrate–cathode distance was fixed at 57 mm. The total plasma pressure for any deposition was kept at 0.04 mbar, while nitrogen partial pressure was varied in the range 0.005–0.02 mbar.

Si-rich layers were fabricated by the co-sputtering of an HfO_2 target topped by Si chips placed on the electron 'race track' with different surface ratios (R_{Si}). R_{Si} is the ratio of the surface of all Si chips to the total surface of the HfO_2 target. To study the thermal stability of the layers, annealing treatments under a nitrogen flow in a conventional furnace at different temperatures, T_A, and durations, t_A, were performed. The deposition and annealing parameters are given in table 1.

Several techniques were used to study the properties of the layers. The thickness of the films was analyzed by means of x-ray reflectometry and spectroscopic ellipsometry and was found to be in the range of 10–14 nm. ATR-FTIR spectra were measured in the range 600–4000 cm^{-1} by means of a 60° Ge Smart Ark accessory inserted in a Nicolet Nexus spectrometer. X-ray diffraction analysis was performed using a Philips XPERT HPD Pro device with Cu Kα radiation (λ = 0.1514 nm) at a fixed grazing angle incidence of 0.5°. An asymmetric grazing geometry was chosen to increase the volume of material interacting with the x-ray beam, as well as to eliminate the contribution from the Si substrate. Cross-sectional specimens were prepared for TEM observations by the standard procedure involving grinding, dimpling and Ar^+ ion beam thinning until electron transparency. The samples were examined by high resolution transmission electron microscopy (HRTEM) on an FEI Tecnai microscope operating at 200 keV equipped with a field emission gun and a spherical aberration corrector. The chemical analysis is performed by electron energy loss spectroscopy (EELS) with a probe of 1 nm used in scanning mode (STEM-EELS) to analyze the composition of the different layers. This technique allows us to construct elemental profiles or mapping of all the elements present in the film.

3. Results and discussion

The effects of the deposition conditions (the power density applied to the HfO_2 cathode, total plasma pressure, cathode–

substrate distance, temperature of substrate and, in the case of Si-rich layers, the number of Si chips topped on the HfO_2 target, i.e. the Si content) as well as the annealing treatment on the properties of pure and Si-rich HfO_2 layers were studied.

3.1. As-deposited pure and N-rich HfO_2 layers

A set of layers has been fabricated with different RFP values at given T_S and vice versa (table 1). First, structural properties of the layers were examined by the XRD method. It was found that as-deposited pure and N-rich HfO_2 layers have similar XRD patterns. Thus the main results and trends will be described for pure HfO_2 layers.

It is known that, when HfO_2 layers have monoclinic structure, the most intense reflections in the range of $2\Theta = 15°–65°$ are detected for (111) ($2\Theta = 28.370°$ and $31.676°$), for (200) ($2\Theta = 34.338°$, $34.665°$ and $35.547°$), and for (220) planes ($2\Theta = 49.593°$, $50.496°$ and $50.914°$) [23]. The decrease of HfO_2 grain sizes results in the broadening of XRD peaks and for the case of amorphous structure only one broad peak in the range of $2\Theta \approx 28°–32°$ is usually observed [18, 19].

XRD patterns of pure and N-rich layers grown with RFP = 0.98 W cm^{-2} at $T_S = 45$ °C were found to be similar and revealed a broad peak in the range of $2\Theta \approx 25°–35°$ with a maximum intensity situated at $2\Theta \approx 32°$ (figure 1(a)). The decrease in RFP values did not lead to a variation of XRD patterns (not shown here). This allows us to suppose that the layers grown at $T_S = 45$ °C were amorphous.

In increasing the T_S value, a narrowing of the XRD peak ($2\Theta \approx 25°–35°$) was observed and accompanied by the shift of its position towards lower 2Θ values (figure 1(a)). This effect is more pronounced for lower RFP values (figure 1(b)). Thus, for the layers grown with RFP = 0.48 W cm^{-2} the XRD peak shifts from $2\Theta \approx 31°$ ($T_S = 100$ °C) (figure 1(b), curve 1) to $2\Theta \approx 28°–29°$ ($T_S = 500$ °C) accompanied by a decrease of its width (figure 1(b), curve 3). This testifies to the formation of HfO_2 grains during the film growth. Usually, their sizes can be estimated using Scherrer's formula [24], but in this case XRD patterns have to be taken in symmetric geometry. Taking into account that, for the asymmetric configuration used in our study, this formula will give overestimated values, the maximal size of the grains was found to be about 4 nm. An appearance of a shoulder at $2\Theta \approx 35°–36°$ (figure 1(b), curve 3, marked by an arrow) was also observed that can be a signature of the grain shape approaching the spherical one.

When $T_S = 500$ °C, but RFP = 0.98 W cm^{-2}, the broadening of the XRD peak $2\Theta \approx 28°–29°$ was observed, while the shoulder at $2\Theta \approx 35°–36°$ was not detected (figure 1(b), curve 4). Such a behavior is due to a decreasing of grain sizes down to an estimated value of 3 nm.

XRD spectra demonstrate that the increase of T_S at given RFP results in the crystallization of HfO_2 layers, whereas the increase of RFP at a given T_S leads to a decrease of HfO_2 grain sizes. Thus the accurate combination of definite deposition conditions (for example, $T_S = 45–100$ °C, RFP = 0.74–0.98 W cm^{-2}) allows for growing amorphous layers.

To confirm such a hypothesis, *ATR experiments* have been performed on the same pure and N-rich layers (figure 2).

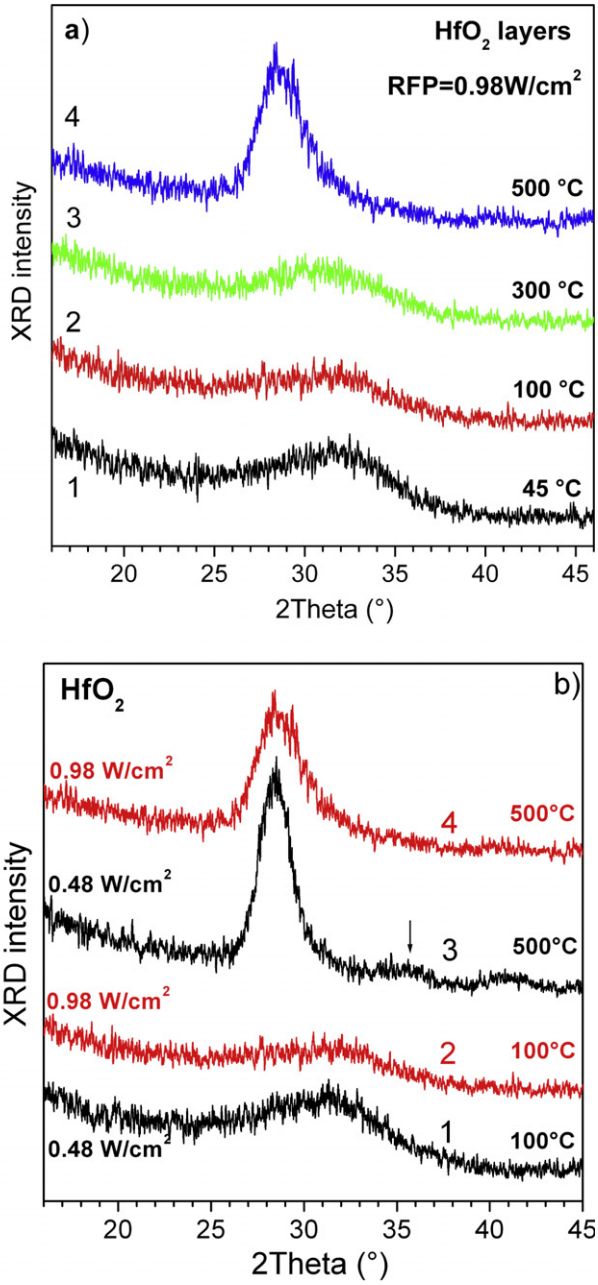

Figure 1. GI-XRD patterns of HfO_2 layers deposited at: (a) $T_S = 45–500$ °C, RFP = 0.98 W cm^{-2}; (b) $T_S = 100$ °C (1, 2) and 500 °C (3, 4); RFP = 0.48 W cm^{-2} (1, 3) and 0.98 W cm^{-2} (2, 4).

The presence of two main vibration bands in the range of 600–800 cm^{-1} and 960–1260 cm^{-1} was revealed. Usually, Hf–O vibration bands are situated in the range of 600–800 cm^{-1} [25, 26]. The information about the crystalline or amorphous nature of the layers can be obtained from the shape and the position of these vibration band(s). When a crystalline HfO_2 phase is present in the layer, well-defined peaks are detected at 770–780 cm^{-1} and 675–685 cm^{-1}. These peaks were detected for HfO_2 films [25, 26] and calculated based on experimental results [27]. At the same time the observation of only one broad band with the maximum around 690–700 cm^{-1} was usually explained by the amorphous nature

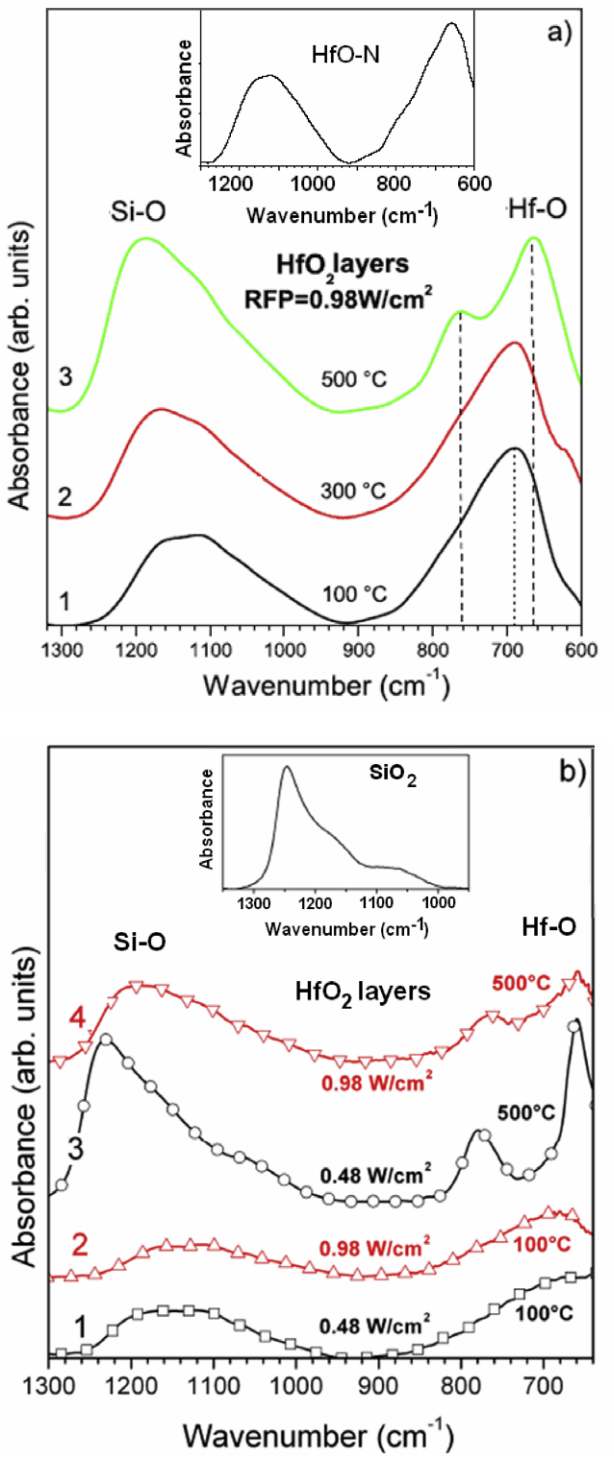

Figure 2. ATR spectra of pure HfO_2 layers deposited at: (a) RFP = 0.98 W cm^{-2}, T_S = 100 °C (1), 300 °C (2) and 500 °C (3). The inset represents ATR spectrum of N-rich HfO_2 layer; (b) RFP = 0.048 (1, 3) and 0.98 (2, 4) W cm^{-2}, T_S = 100 °C (1, 2) and 500 °C (3, 4). The inset represents ATR spectrum of 2 nm thick SiO_2 layer.

of the layers [25]. Note that the peak at 770–780 cm^{-1} is considered as a signature of the monoclinic HfO_2 phase [25].

ATR spectra of pure and N-rich HfO_2 layers deposited at T_S = 45 °C were found to be similar (figure 2(a)). A broad Hf–O vibration band was detected at 690 cm^{-1} for pure layers as well as N-rich ones. The increase of T_S up to 300 °C did change neither the shape nor the position of this band (figure 2). This means that the layers fabricated at $T_S \leqslant 300$ °C can be considered as amorphous ones. Further increase of T_S up to 500 °C results in the transformation of the Hf–O band: two peaks situated at about 770 and at 665 cm^{-1} were detected (figure 2), which indicated the formation of a crystalline HfO_2 phase during the growth. Such an evolution is in agreement with previous XRD data described above (figure 1(a)).

ATR spectra of as-deposited layers reveal also the presence of another vibration band in the range of 900–1250 cm^{-1} (figures 2(a) and (b)). This band is ascribed to LO_3 and TO_3 Si–O phonon modes and its appearance is usually caused by the formation of an SiO_x interfacial layer as previously reported in [3–5, 11, 13, 20]. The peak position of the Si–O band depends on the deposition conditions. For the layers deposited at T_S = 100 °C, it was situated at 1160 cm^{-1} and shifted towards 1100 cm^{-1} with the increase in RFP value (figure 2(b), curves 1 and 2).

The increase of T_S up to 500 °C led to the shift of the Si–O band peak position to higher wavenumbers up to 1200 cm^{-1} (figure 2(b), curve 3), which corresponds to stoichiometric SiO_2 (figure 2(b), inset). Similar spectra were observed for SiO_2 by Frank *et al* [26] and the evolution of the shape and peak position of the Si–O band was explained by the variation of thickness and composition of the silicon oxide layer. The shift of the Si–O peak position to the lower wavenumber side was ascribed to a formation of a sub-stoichiometric silicon oxide layer as well as to the decrease of the layer thickness [26]. This can explain the behavior of the Si–O band caused by an interfacial SiO_x layer in the present study with the variation of the RFP and T_S.

It should be noted that, for N-rich layers deposited with high nitrogen content in the plasma, the peak position of this band was found to be shifted to the lower wavenumber side (figure 2(a), inset), which can be considered as the formation of an SiO_xN_y interfacial layer (this will be demonstrated below).

ATR results showed that pure and N-rich HfO_2 layers grown at 45–100 °C can be considered as amorphous. To confirm XRD ant ATR results, as well as to obtain additional information about the structure and homogeneity of HfO_2 layers, *TEM observations* were also performed for the same samples.

Cross sections of pure and N-rich HfO_2 layers, studied by XRD and ATR methods and described above, were prepared for HRTEM observations. The formation of an interfacial layer occurs during the deposition for pure as well as for N-rich layers. For the case of pure layers the thickness of interfacial layers is 2.5 nm for the film grown at T_S = 45 °C with RFP = 0.74 W cm^{-2} (figure 3(a)). The increase of the RFP value to 0.98 W cm^{-2} at a given T_S leads to the increase of the total thickness of the film from 9.5 to 11 nm (figures 3(a) and (b)) without any noticeable effect on the interface Si/HfO_2. STEM-EELS analyses (not shown) performed in both samples show that the layers are composed of pure HfO_2, while the interfacial layer is SiO_x. As a consequence, the clear contrast observed in the HfO_2 layer in the HRTEM images is due to porosity.

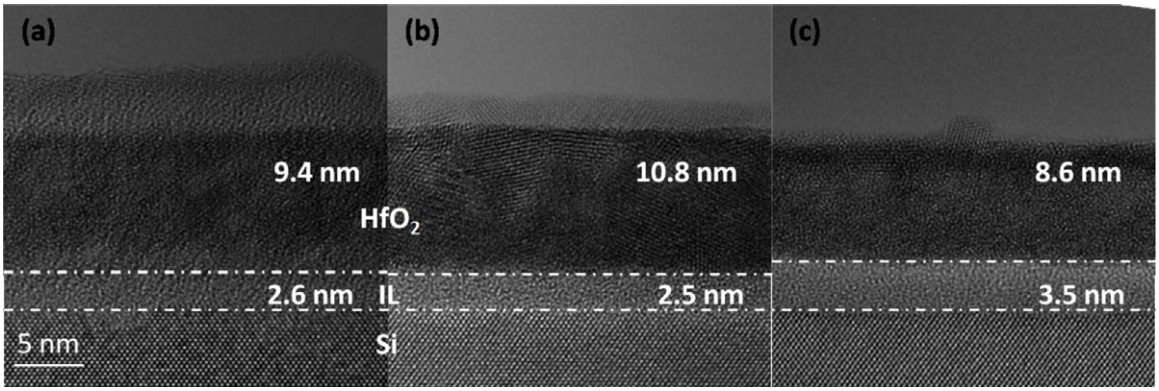

Figure 3. TEM cross-sectional images of pure HfO_2 layers as-deposited ((a), (b)) and annealed at 800 °C for 15 min (c). Deposition conditions: $T_S = 45$ °C, RFP = 0.74 W cm^{-2} ((a), (c)) and 0.98 W cm^{-2} (b). IL = interfacial SiO_x layer.

The comparison of the images presented in figures 3(a) and (b) also shows that the HfO_2 layer grown at $T_S = 45$ °C with RFP = 0.98 W cm^{-2} is more crystalline than the layer deposited with RFP = 0.74 W cm^{-2}. One of the possible reasons for this difference in terms of thickness and crystallinity is the deposition rate. It was about 4 nm min^{-1} for RFP = 0.98 W cm^{-2} against 1.5 nm min^{-1} for RFP = 0.74 W cm^{-2}. Going further, one can say that this was one of the criteria for the choice of RFP = 0.74 W cm^{-2} for the fabrication of future HfO_2-based films.

STEM-EELS analysis of N-rich layers revealed the enrichment of the interfacial layer by nitrogen. The increase of nitrogen partial pressure in argon–nitrogen plasma from 0.005 mbar to 0.02 mbar led to the increase of the [N]/[O] ratio from 0.1 to 0.25. Such analysis confirms the ATR data and allows us to conclude that the interfacial layer is SiO_xN_y. At the same time it is interesting that in the HfO_2 layer itself nitrogen was not detected whatever the nitrogen content in plasma. This fact can explain the similarity of ATR spectra observed for pure and N-rich layers.

RF magnetron sputtering of a pure HfO_2 target allows us to fabricate amorphous pure and N-rich HfO_2 layers at given deposition conditions. Nevertheless, these layers systematically present a 2.5 nm thick interfacial layer. However, the formation of an SiO_xN_{1-x} layer is preferable in terms of electrical application of the HfO_2-based layers due to the lower content of defects in comparison with the SiO_2 interfacial layer. Moreover it is considered that N-rich layers have to demonstrate better thermal stability than their pure counterparts [17, 21].

3.2. Annealed pure and N-rich HfO_2 layers

To study thermal stability of pure and N-rich HfO_2 layers, an annealing in nitrogen flow at $T_A = 600$–1100 °C and $t_A = 5$–60 min was performed. The results will only be presented for the layer grown at RFP = 0.74 W cm^{-2} and $T_S = 100$ °C (figures 4(a) and (b), curve 1) and found to be homogeneous and amorphous after deposition (figure 3(a)).

Different behavior of Si–O and Hf–O vibration bands is observed with annealing treatment. Thus, an initial broad Si–O band, situated at about 1100 cm^{-1} (figures 4(a) and (b)) and considered as a feature of the SiO_x layer, changes its shape and shifts towards 1180 cm^{-1} after annealing at $T_A = 600$ °C during 15 min (figure 4(a)). Its separation on LO_3 and TO_3 Si–O phonon modes occurs at $T_A = 800$ °C. These two phonon peaks are due to the Si oxide interfacial layer with the Si substrate [28]. The increase of T_A at given t_A (figure 4(a)) or vice versa (figure 4(b)) results in the shift of LO_3 and TO_3 phonon modes towards those observed for stoichiometric SiO_2 (1230 cm^{-1} and 1070 cm^{-1}, respectively). This evolution of the Si–O band can be explained by an improving of the SiO_x interfacial layer structure and its transformation to stoichiometric SiO_2. The latter requires a diffusion of oxygen towards the layer/substrate interface that occurs preferably from the HfO_2 layer close to the HfO_2/Si interface as was shown by Jiang *et al* [29].

Concerning now the Hf–O vibration band, its evolution is starting at lower T_A after long-time annealing (more that 15 min) (figures 4(a) and (b)) and is accompanied by an appearance of a shoulder at about 770 cm^{-1} (figure 4(b), curves 2 and 3) transformed to a well-defined band (curves 4 and 5). The similar behavior is observed after short-time annealing (less than 5–10 min) for higher annealing temperatures (more than 900 °C) (figure 4(a), curves 4 and 5). Two separate bands at 770 and 680 cm^{-1} are detected, that confirm the layer crystallization. These results show that the crystallization of the HfO_2 layer depends strongly on both annealing time and temperature. For the layers fabricated at RFP = 0.74 W cm^{-2} and $T_S = 100$ °C, the crystallization needs a longer annealing time and a higher temperature.

It should be noted that N-rich HfO_2 layers become crystallized at lower T_A and/or t_A as shown in figure 4(c). Moreover, the decrease of the [N]/[O] ratio was observed. This can be explained by the increasing oxygen content in the layers due to their porosity (as was demonstrated by TEM analysis) and, as a consequence, their easy crystallization due to oxidation.

The XRD study of HfO_2 layers versus annealing treatment confirms the ATR results. For pure layers fabricated with the highest RFP value, the evolution of XRD patterns was found only after annealing at $T_A = 800$ °C during 15 min (figure 5). It led to a transformation of the shape of the broad XRD peak

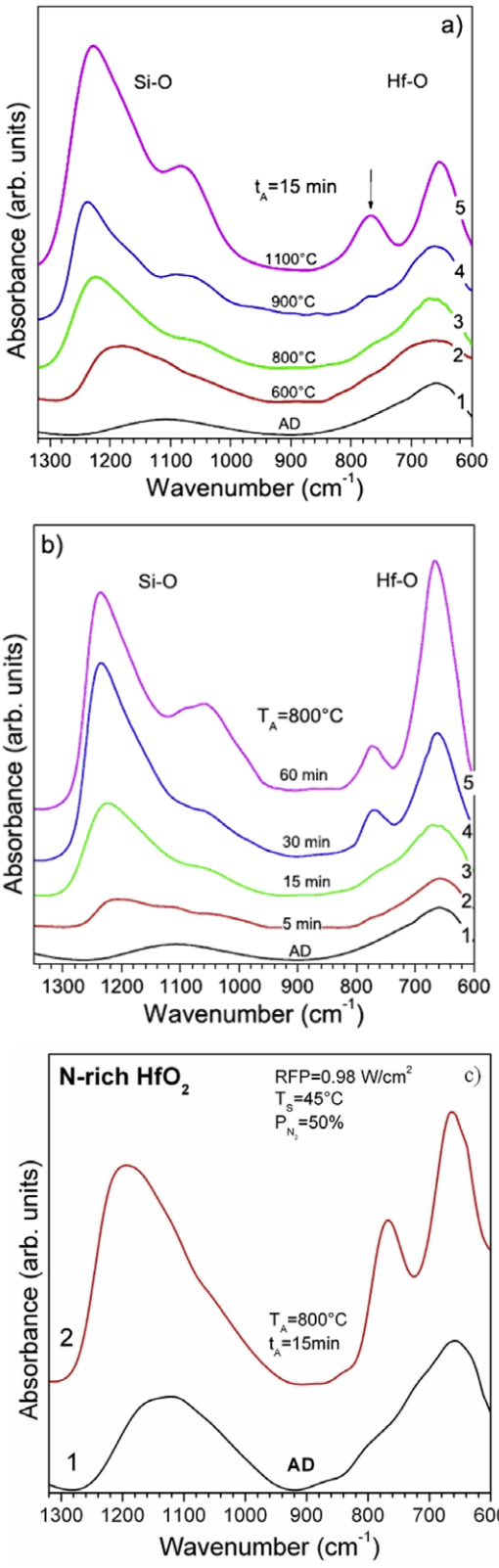

Figure 4. The evolution of ATR spectra of pure ((a), (b)) and N-rich (c) HfO_2 layers with annealing temperature ((a), (c)) and time (b). (a) As-deposited (AD) (1), annealed at $T_A = 600\,^{\circ}C$ (2), 800 °C (3), 900 °C (4) and 1100 °C (5); $t_A = 15$ min. (b) As-deposited (AD) (1), annealed during 5 min (2), 15 min (3), 30 min (4) and 60 min (5). $T_A = 800\,^{\circ}C$. For both graphs curves 1 and curves 3 correspond to each other. (c) As-deposited (AD) (1) and annealed at $T_A = 800\,^{\circ}C$, $t_A = 15$ min (2). Deposition conditions: RFP = 0.74 W cm^{-2} ((a), (b)) and 0.98 W cm^{-2} (c), $T_S = 45\,^{\circ}C$.

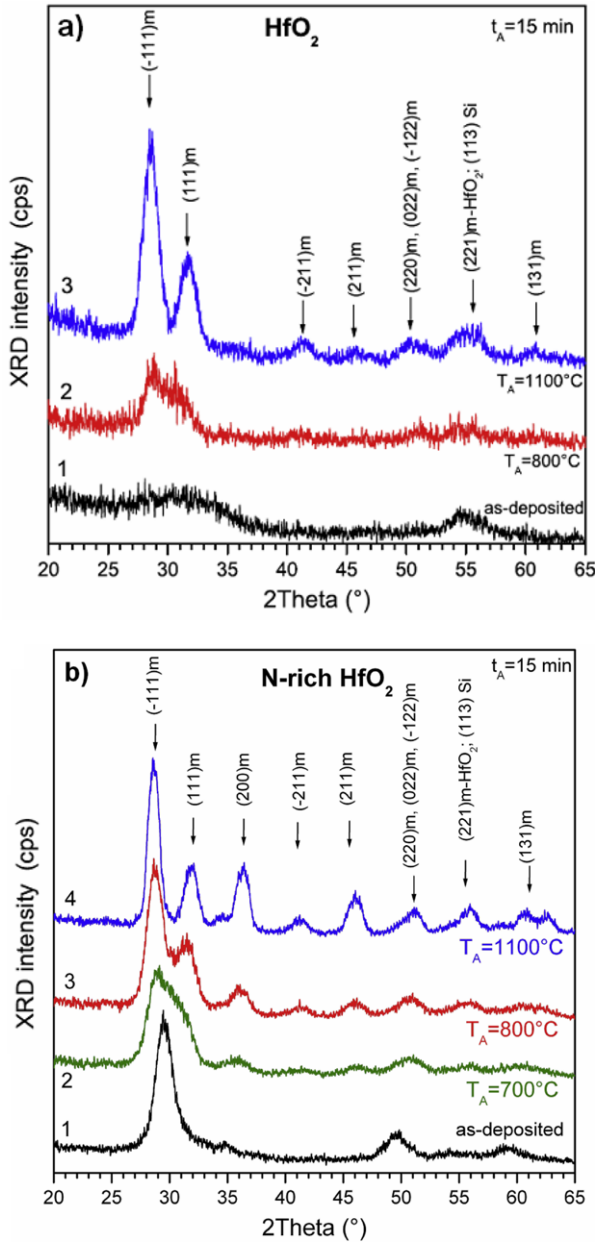

Figure 5. (a) XRD patterns measured for pure HfO_2 layers: as-deposited (1), annealed at $T_A = 800\,^{\circ}C$ (2) and 1100 °C (3) during 15 min. ATR spectra of these layers are shown in figure 4; deposition conditions: RFP = 0.74 W cm^{-2}, $T_S = 45\,^{\circ}C$. (b) XRD patterns measured for N-rich HfO_2 layers: as-deposited (1), annealed at $T_A = 700\,^{\circ}C$ (2), 800 °C (3) and 1100 °C (4). Annealing time for both figures was 15 min. Deposition conditions: RFP = 0.98 W cm^{-2}, $T_S = 45\,^{\circ}C$, nitrogen partial pressure is 0.02 mbar.

and an appearance of two overlapped peaks at $2\Theta \approx 28.5°$ and 31.7°. The increase of annealing time and/or temperature resulted in the increase in the intensity of these peaks with their concomitant narrowing as well as an appearance of some peaks in the range of $2\Theta = 40°$–$65°$. As one can see from figure 5, for the layer annealed at $T_A = 1100\,^{\circ}C$ during 15 min, the most intense XRD peaks were found at $2\Theta \approx 28.5°$ and 31.7°, corresponding to the (111) plane of monoclinic HfO_2.

The diffraction from (211), (220) and (311) planes was also observed in the range of $2\Theta = 40°$–$65°$. Note that the peak at $2\Theta \approx 55°$ overlaps with the peak corresponding to the (113) plane of the Si substrate, usually observed for the Si substrate itself used in this study and detected also for as-deposited layers.

The XRD study of N-rich layers confirmed the ATR results. It was found that crystallization of these layers begins at $T_A = 700\,°C$ after 5 min annealing, while a clear formation of the monoclinic phase at $T_A = 800\,°C$ and $t_A = 15$ min was detected, in contrast to pure layers when the crystallization process was found to be started after longer annealing treatment. The TEM image obtained for the pure HfO_2 layer annealed at $T_A = 800\,°C$ during 15 min shows that such a treatment results only in the increase of the thickness of the interfacial layer from 2.5 to 3.5 nm, while the HfO_2 film is still amorphous (figure 3(c)).

The analysis of the properties of pure and N-rich HfO_2 layers showed that unfortunately it is impossible to avoid the formation of interfacial SiO_2 or SiO_xN_{1-x} layers when films were grown from a pure HfO_2 target. However, some specific deposition conditions were found to be suitable to fabricate homogeneous amorphous HfO_2 films. The different annealing treatment allowed us to find a window in the annealing conditions ($T_A = 800\,°C$ and $t_A \leqslant 15$ min) when the HfO_2 layer conserves its amorphous structure, whereas the SiO_x interfacial layer improves its stoichiometry. This is one of the key points for the application of magnetron-sputtered HfO_2 as a gate material. At the same time, in most of the cases, the formation of a thick interfacial layer occurs. This requires us to determine the optimized parameters allowing us to control or to avoid the formation of this layer during either the deposition or the annealing process. One of these parameters consists of the incorporation of silicon in the HfO_2 matrix.

3.3. Si-rich layers

3.3.1. The effect of R_{Si} on the structural properties of the films. To study the effect of Si incorporation on the properties of the films when the R_{Si} value was varied in the range of 3–12%, Si-rich samples were fabricated with the same deposition parameters as their Si-free counterparts described above. The films were deposited as in pure argon plasma to obtain HfSiO films, as in mixed argon–nitrogen plasma to have HfSiON films. As was demonstrated above, the high content of nitrogen in plasma resulted in the worsening of thermal stability of the films. In this case to discriminate the effect of Si and N on the thermal stability of the films, the nitrogen partial pressure was kept at 0.005 mbar and at 0.02 mbar and the films were grown with $R_{Si} = 3$–12%. In general, it was observed that Si plays a more important role in the stability of the amorphous structure of the films and this will be shown below.

The comparison of cross-section TEM images of as-deposited N-rich HfO_2 and Si-rich N-HfO_2 films (HfSiON), fabricated with $R_S = 12\%$, shows a decrease of the interlayer thickness from about 2.5 nm ($R_{Si} = 0\%$, figure 3(a)) to 1 nm ($R_{Si} = 12\%$, figure 6(a)) and a decrease of the crystallinity with the Si content (figure 6). This allows us to conclude that a decrease of interfacial layer thickness for Si-rich layers occurs due to Si incorporation. In addition, the presence of Si in the layer is responsible for the amorphous nature of the high-k HfSiON layer, compared to HfON ones elaborated in the same deposition conditions.

A similar effect was observed for the HfSiO layers. The silica nature of the interfacial layer is confirmed by STEM-EELS analysis (see figure 6(b)).

The Si content in the HfSiO layer is around 20%, as measured on the STEM-EELS elemental profiles (figure 6(b)). In addition, the presence of a high amount of N (around 20%) has been detected in the interfacial layer with an extension towards the first half of the HfSiON layer. In this case the incorporation of nitrogen into the layer is governed by silicon. Some clear contrast is also visible in the HfSiO layers imaged in HRTEM (figure 6(a)) and is due to Si-rich areas, as will be shown for the annealed samples (see section 3.3.2).

TEM results described above are in agreement with XRD patterns obtained for Si-rich layers. As one can see from figure 7(a), the increase of R_{Si} results in the decrease of the intensity as well as in the broadening of the XRD peak situated at $2\Theta = 31°$–$32°$.

It is worth noting that, for Si-rich layers, XRD peak positions are known only for tetragonal $HfSiO_4$ material, for which the most intense reflections in the range of $2\Theta = 15°$–$40°$ can be detected at $2\Theta = 20.05°$ (for the (101) plane), $2\Theta = 27.08°$ (for the (200) plane) and $2\Theta = 35.66°$ (for the (112) plane) [30]. Moreover, for the case of amorphous layers, the main XRD peak is usually observed in the same range as for pure HfO_2 counterparts. Thus XRD patterns presented in figure 7(a) can be explained by an increase of the contribution of the amorphous phase with R_{Si} increase since the thickness of the layers was kept constant. Such behavior was observed not only for the thin layers (figure 7(a)), but for their thicker counterparts (figure 7(b)). As one can see, thick pure HfO_2 layers contain a monoclinic HfO_2 phase reflected by two peaks corresponded to the (111) plane. At the same time XRD patterns of Si-rich layers deposited with $R_{Si} = 6\%$ and 12% demonstrate only one broad peak situated at about $2\Theta \approx 31°$–$32°$ (figure 7(b)). This means that Si incorporation into the HfO_2 matrix results in the conservation of the amorphous nature of the layers not only for thin films but also for thicker ones.

To obtain the information about chemical composition of the films versus R_{Si}, ATR spectra were studied for the same samples and they are presented in figure 8. Unfortunately, only a few data about vibration bands for Si-rich HfO_2 layers are available up to now and most of them were obtained for thick films prepared by vapor-based techniques [15, 31]. In such a case, the infrared absorption band corresponding to the Hf–Si–O stretching vibration was observed between 888 and 1004 cm^{-1}. For the layers prepared by the MOCVD technique, it was shown that Si incorporation into the HfO_2 matrix leads to the appearance of the broad band in the 800–1100 cm^{-1} spectral range, while the increase of Si content in the layers from 10 to 60 at.% results in the shift of peak position from 940 to 980 cm^{-1} [15].

The spectra obtained for our layers grown with $R_{Si} = 3$–6% are similar to the spectra for pure HfO_2 layers: both Hf–O

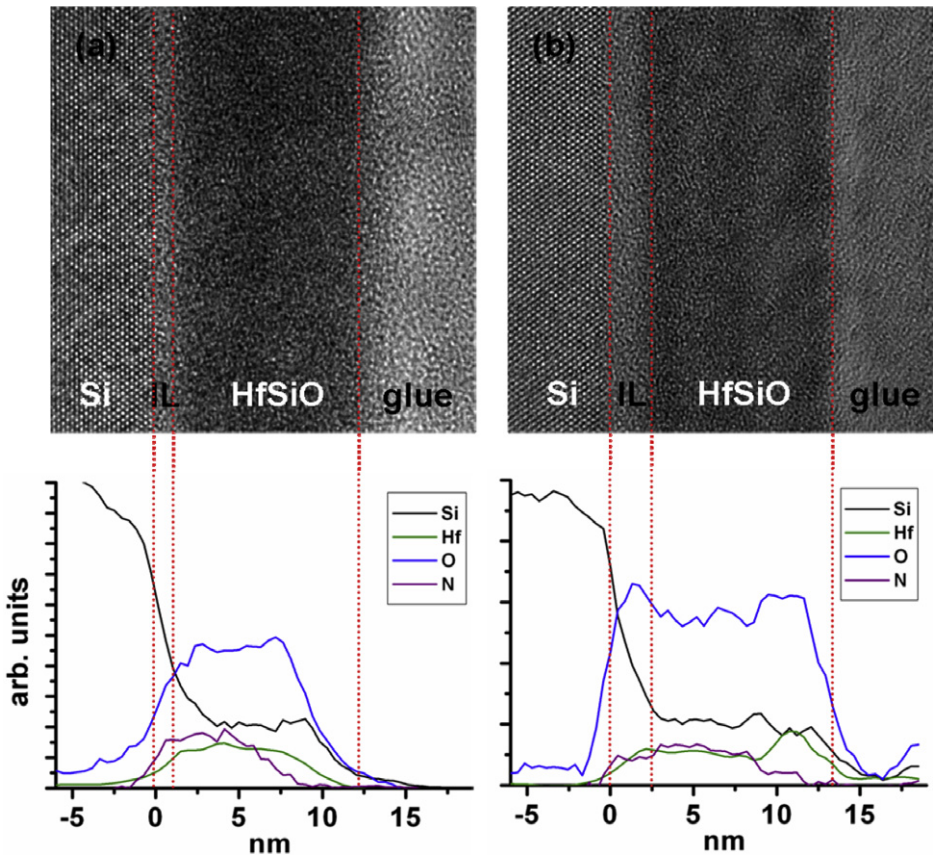

Figure 6. Cross-sectional HRTEM images and STEM-EELS elemental profiles of HfSiO layers ($R_{Si} = 12\%$): (a) as-deposited and (b) annealed 15 min at 800 °C, fabricated with $T_S = 45$ °C, RFP = 0.74 W cm^{-2}.

and Si–O vibrational bands were detected (figure 8(a)). The peak position of the Hf–O band was found to be situated at about 680–700 cm^{-1}, while the peak position of the Si–O related band was shifted to lower wavenumbers. This can be due to the formation of SiO_x [26] or silicate interfacial layer with lower thickness [15], which is confirmed by TEM study (figure 6). The absence of any well-defined Hf–O related vibration band at 770–780 cm^{-1} indicates the amorphous nature of the layers.

ATR spectra of the layers deposited with $R_{Si} = 12\%$ demonstrate the presence of a broad band peaked at 1050 cm^{-1} with a shoulder at about 900 cm^{-1} with a tail up to 600 cm^{-1} (figure 8(b)). It was observed that an increase of T_S up to 500 °C did not lead to transformation of this band. Moreover no Si–O vibration band was detected in contrast to the pure HfO_2 layer grown at the same deposition conditions (figure 2). This allows us to conclude that whatever T_S value is used in this study, the formation of a stable amorphous Si-rich HfO_2 matrix occurs during deposition (figure 8(b)).

3.3.2. The effect of annealing treatment on the properties of Si-rich HfO_2 layers. An annealing of the layers, grown with $R_{Si} = 12\%$ and $T_S = 45$ °C, at $T_A = 800$ °C for 15 min leads to the shift of the broad ATR peak from 1050 to 1070 cm^{-1} while the lower wavenumber part of the ATR spectrum does not change (figure 10). Such a shift should be caused by a transformation of the Si–O bonds. At the same time the increase of T_A up to 1000 °C does not lead to the crystallization of the layers since neither a shoulder nor a peak at 770–780 cm^{-1} were observed after annealing (figure 10). Similar behavior was also found for the layers deposited with higher T_S and RFP. These data give evidence that the incorporation of silicon into an HfO_2 matrix improves thermal stability of the layers. It is known that Si–O bonds are characterized by high flexibility [4] which allows conserving the amorphous nature of fused silica. And this Si–O bond ability was supposed to govern the stability of the amorphous nature of HfSiO films for high-temperature annealing.

For the films fabricated with $R_{Si} = 12\%$, the HRTEM images show that the HfSiO layer remains amorphous after annealing (figure 6(b)). The interfacial layer, labeled IL, is now 2.5 nm thick instead of 1 nm for the as-deposited layer. The Si content in the HfSiO layer, measured by STEM-EELS, is the same as for the as-deposited layer (20%, see figure 6(a)). Nitrogen is again present in the interfacial and HfSiO layers, with an amount of 10% and has diffused in the whole HfSiO layer. Some clear contrast is observed in the HREM images and can be attributed to either porosity as in the case of pure HfO_2 layers or the presence of regions lighter than HfO_2 in terms of atomic density and atomic number. As expected, these regions appear dark in annular dark field images, where the contrast is mainly due to the square of the atomic number

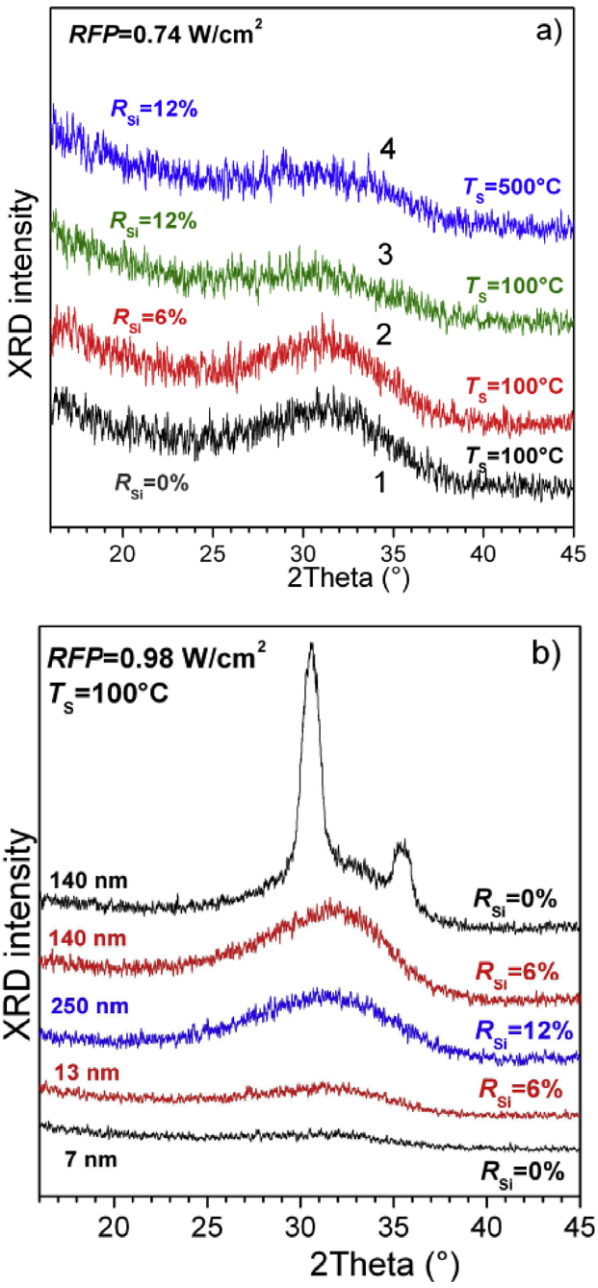

Figure 7. (a) GI-XRD patterns of as-deposited HfO_2-based layers versus R_{Si} and thickness of the layer. $R_{Si} = 0\%$ (1), 6% (2) and 12% (3, 4); $T_S = 100\,^{\circ}C$ (1–3) and 500 °C (4); RFP = 0.74 W cm^{-2}. The thickness of all the layers is about 14 nm. (b) GI-XRD patterns of as-deposited HfO_2-based layers of different thicknesses grown with different R_{Si} values. RFP = 0.74 W cm^{-2}, $T_S = 100\,^{\circ}C$. The values of R_{Si} and thicknesses of the layers are mentioned in the figure.

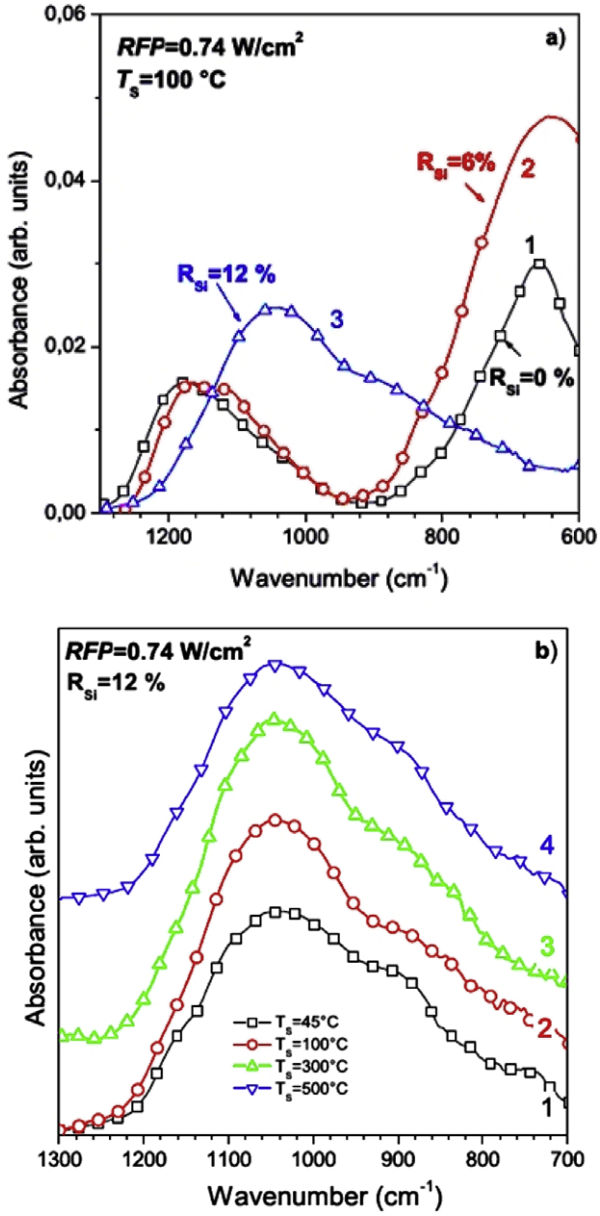

Figure 8. ATR spectra of (a) HfO-based layers versus R_{Si} (RFP = 0.74 W cm^{-2}, $T_S = 100\,^{\circ}C$) and (b) HfSiO layers versus T_S ($R_{Si} = 12\%$, RFP = 0.74 W cm^{-2}). T_S values are mentioned in the figure.

of the elements (figure 9(a)). The associated STEM-EELS mapping of Si (figure 9(b)) shows clearly that these regions are composed of Si-rich regions.

For Si-rich layers grown with $R_{Si} \leqslant 6\%$, the presence of well-defined Hf–O and Si–O bonds was observed. The last one can be caused not only by an interfacial SiO_x layer but also by the formation of Si-rich areas inside the Hf-based layer. This assumption was confirmed by STEM-EELS data where the energy loss near-edge structure (ELNES) of the Si K edge shows that Si is bonded with O across the layer (not shown here). It is obvious that different phases (SiO_2-rich and HfO_2-rich one) will demonstrate different reactions on the annealing treatment. Indeed, if the layer will contain HfO_2-rich regions, after annealing at $T_A \geqslant 850\,^{\circ}C$ they will be crystalline as was observed for the pure HfO_2 layers. An appearance of a well-defined Hf–O band will be therefore expected in the ATR spectra. Simultaneously, the transformation of an Si–O bond will occur, leading to the shift of the Si–O vibration band to higher wavenumbers. In this case ATR spectra will be similar to the one presented by curve 2 in figure 4 for annealed HfO_2 layers.

It is known that Si incorporation into an HfO_2 matrix leads to the formation not only of O–Si–O and O–Hf–O, but

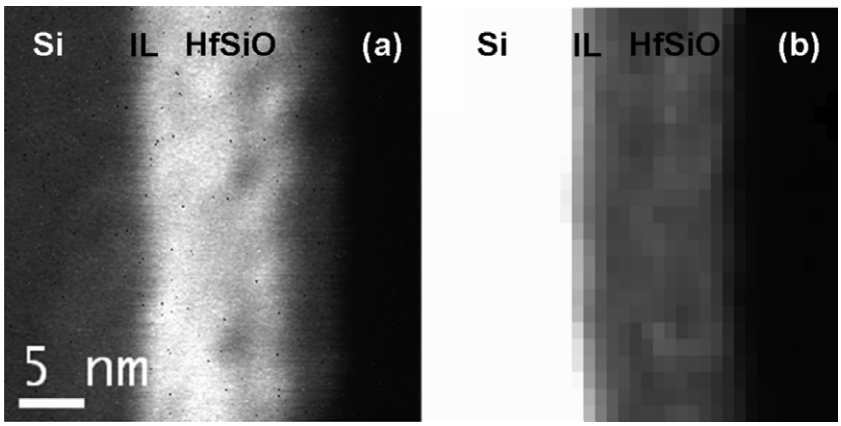

Figure 9. (a) Annular dark-field image and (b) associated STEM-EELS elemental mapping of Si in the Si substrate/HfSiO layer.

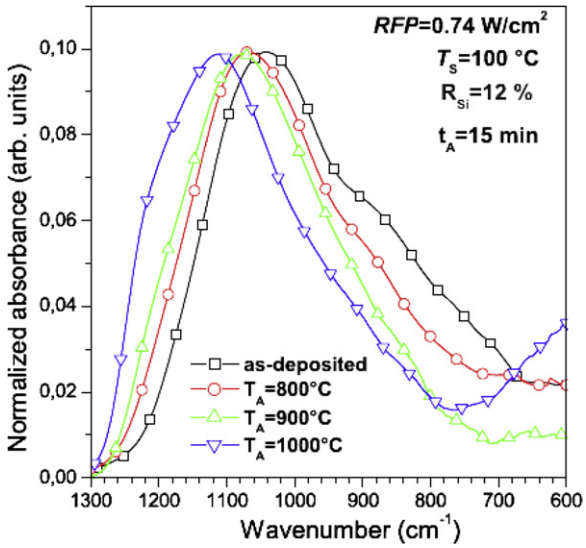

Figure 10. Evolution of ATR spectra of HfSiO layer deposited with $R_S = 12\%$, RFP = 0.74 W cm^{-2}. $T_S = 100\,^{\circ}$C. Annealing parameters are mentioned in the figure.

also Hf–O–Si bonds rather than Hf–Si ones [32]. In this case the ATR spectrum is similar to the one presented by curve 2 in figure 5. However, when Si content is high enough, the preferable formation of Hf–Si–O bonds occurs as shown in figure 8(a) (curve 3). It is possible that in our case for the layers grown with $R_{Si} = 12\%$ the formation of Hf–Si–O and O–Si–O bonds takes place rather than O–Hf–O ones. This correlates with the absence of a related vibration band in the range of 600–800 cm^{-1}. In this case one can think that the layer grown with $R_{Si} = 12\%$ can be considered as a layer containing HfO_2, HfSiO and SiO_x phases and this should explain the appearance of some contrast in the upper part of the film (figure 6(c)). At the same time the layer grown with $R_{Si} = 6\%$ can be considered as the layer consisting of SiO_x, HfO_x and, to a lower extent, HfSiO phases. The annealing stimulates the transformation of all the bonds. However, the Hf–O well-defined peak should appear only if the formation of the HfO_2-rich region will occur. However, any Hf–O peaks were not revealed in ATR spectra in the range 600–800 cm^{-1} (figure 10). This can be explained by the transformation of Si–O bonds resulting in the shift of the peak position of the main bands to the higher wavenumber side due to an increasing contribution of the LO_3 phonon mode of Si–O bonds. It is possible that in this case not only an SiO_2 interfacial layer is formed, but also a phase separation of the HfSiO matrix takes place. The similar effect was observed for ZrSiO layers and explained by the separation of the ZrSiO matrix on ZrO_2 and SiO_2 phases [32]. Based on the assumption about the similar nature of Zr and Hf, it was supposed also that their silicates have to demonstrate similar properties [4, 32]. In our case, one can assume that, besides the formation (or the transformation) of the SiO_2 interfacial layer, the phase separation can occur due to high-temperature annealing. As one can see from figure 10, after annealing at 1000 °C the appearance of the shoulder in the range 600–700 cm^{-1} (or the increase of the intensity) takes place (figure 10). This can be explained by a formation of the HfO_2 phase in annealed layers and requires further structural investigation. Anyway, these HfSiO layers, which remain amorphous after annealing and show a very thin (1 nm) SiO_x interfacial layer, are very promising for microelectronic applications. The investigation of the effect of the deposition conditions and annealing treatment on electrical properties of HfO_2-based layers is actually in progress.

4. Conclusion

Pure and Si-rich HfO_2 layers have been fabricated by RF magnetron sputtering of an HfO_2 target (pure and topped by Si chips) in argon plasma. The effect of the deposition parameters and annealing treatment on the properties of the layers had been investigated by means of x-ray diffraction, infrared absorption spectroscopy and high resolution transmission electron microscopy. It was demonstrated that the increase of the RFP value up to 0.98 W cm^{-2} at $T_S = 45$–$300\,^{\circ}$C allows us to improve the thermal stability of pure HfO_2 layers. The formation of an interfacial SiO_x layer with a thickness of 2.5 nm was observed. It is shown that the incorporation of Si into an HfO_2 matrix leads to the decrease of the interfacial layer thickness to 1 nm and improves the thermal stability of the layers. These results open some perspectives for the RF

magnetron sputtering technique in the production of thermally stable HfO_2-based layers for various applications. The next step concerns the electrical characteristics of some of the optimized layers to confirm their potential applications for the next-generation devices using high-k dielectrics such as Si-based nanomemories.

Acknowledgments

This work is supported by the French National Research Agency (ANR) through the Nanoscience and Nanotechnology Program (NOMAD Project no. ANR-07-NANO-022-02) and, for one of the authors, by the Region Basse Normandie through the CPER project—Nanoscience axe (2007–2013).

References

[1] Wilk G D and Wallace R M 1999 *Appl. Phys. Lett.* **74** 2854
[2] Wilk G D and Wallace R M 2000 *Appl. Phys. Lett.* **76** 112
[3] Wilk G D, Wallace R M and Anthony J M 2000 *J. Appl. Phys.* **87** 484
[4] Wilk G D, Wallace R M and Anthony J M 2001 *J. Appl. Phys.* **89** 5243
[5] Houssa M, Pantisano L, Degraeve R, Schram T, Pourtois G, De Gendt S, Groeseneken G and Heyns M M 2006 *Mater. Sci. Eng.* R **51** 37
[6] Krug C and Lucovsky G 2004 *J. Vac. Sci. Technol.* A **22** 1301
[7] Pant G, Gnade A, Kim M J, Wallace R M, Gnade B E, Quevedo-Lopez M A, Kirsch P D and Krishnan S 2006 *Appl. Phys. Lett.* **89** 032904
[8] Mitchell D R G, Aidla A and Aarik J 2006 *Appl. Surf. Sci.* **253** 606
[9] Gutowski M, Jaffe J E, Liu C-L, Stoker M, Hegde R I, Rai R S and Tobin P J 2002 *Appl. Phys. Lett.* **80** 1897
[10] Kato H, Nango T, Miyagawa T, Katagiri T, Seol K S and Ohki Y 2002 *J. Appl. Phys.* **92** 1106
[11] Kim J-H, Ignatova V A and Weisheit M 2009 *Microelectron. Eng.* **86** 357
[12] Dey S K, Das A, Tsai M, Gu D, Flyod M, Carpenter R W, De Waard H, Werkhoven C and Marcus S 2004 *J. Appl. Phys.* **95** 5042
[13] Maunoury C *et al* 2007 *J. Appl. Phys.* **101** 034112
[14] Park B K, Park J, Cho M, Hwang C S, Oh K, Han Y and Yang D Y 2002 *Appl. Phys. Lett.* **80** 2368
[15] Lui M, Zhu L Q, He G, Wang Z M, Wu J X, Zhang J-Y, Liaw I, Fang Q and Boyd I W 2007 *Appl. Surf. Sci.* **253** 7869
[16] Yamamoto K, Hayashi S, Kubota M and Niwa M 2002 *Appl. Phys. Lett.* **81** 2053
[17] He G, Fang Q and Zang L D 2006 *Mater. Sci. Semicond. Process.* **9** 870
[18] Pereira L, Marques A, Águas H, Nedev N, Georgiev S, Fortunato E and Martins R 2004 *Mater. Sci. Eng.* B **109** 89
[19] Feng L-P, Liu Z-T and Shen Y-M 2009 *Vacuum* **83** 902
[20] Gourbilleau F, Khomenkova L, Dufour C, Coulon P-E and Bonafos C 2009 HfO_2-based Thin Films Deposited by Magnetron Sputtering *Materials and Physics for Nonvolatile Memories* (*Mater. Res. Soc. Symp. Proc.*) vol 1160, ed Y Fujisaki, R Waser, T Li and C Bonafos, Warrendale, PA pp 1160-H05–8
[21] Visokay M R, Chambers J J, Rotondaro A L P, Shanware A and Colombo L 2002 *Appl. Phys. Lett.* **80** 3183
[22] Beyers R 1984 *J. Appl. Phys.* **56** 147
[23] Joint Committee on Powder Diffraction Standards (JCPDS) No. 78-0050
[24] Warren B E 1990 *X-Rays Diffraction* (New York: Dover)
[25] Nguyen N V, Davydov A V, Chandler-Horowitz D and Frank M F 2005 *Appl. Phys. Lett.* **87** 192903
[26] Frank M M, Sayan S, Dörmann S, Emge T J, Wielunski L S, Garfunkel E and Chabal Y J 2004 *Mater. Sci. Eng.* B **109** 6
[27] Zhao X and Vanderbilt D 2002 *Phys. Rev.* B **65** 233106
[28] Roy Chowdhuri A, Jin D-U, Rosado J and Takoudis C G 2003 *Phys. Rev.* B **67** 245305
[29] Jiang R, Xie E Q and Wang Z F 2007 *J. Mater. Sci.* **42** 7343
[30] Joint Committee on Powder Diffraction Standards (JCPDS) No. 75-1628
[31] Cosnier V, Olivier M, Theret G and Andre B 2001 *J. Vac. Sci. Technol.* A **19** 2267
[32] Rayner G B Jr, Kang D, Hinkle C L, Hong J G and Lucovsky G 2004 *Microelectron. Eng.* **72** 304